



On the role of trend and variability of hydroxyl radical (OH) in the global methane budget

Yuanhong Zhao¹, Marielle Saunois¹, Philippe Bousquet¹, Xin Lin^{1*}, Antoine Berchet¹, Michaela I. Hegglin², Josep G. Canadell³, Robert B. Jackson⁴, Makoto Deushi⁵, Patrick Jöckel⁶, Douglas Kinnison⁷, Ole Kirner⁸, Sarah Strode^{9,10}, Simone Tilmes¹¹, Edward J. Dlugokencky¹², and Bo Zheng¹

5

¹ Laboratoire des Sciences du Climat et de l'Environnement, LSCE-IPSL (CEA-CNRS-UVSQ), Université Paris-Saclay, 91191 Gif-sur-Yvette, France

² Department of Meteorology, University of Reading, Earley Gate, Reading RG6 6BB, United Kingdom

10 ³ Global Carbon Project, CSIRO Oceans and Atmosphere, Canberra, Australian Capital Territory 2601, Australia

⁴ Earth System Science Department, Woods Institute for the Environment, and Precourt Institute for Energy, Stanford University, Stanford, CA 94305, USA

⁵ Meteorological Research Institute, 1-1 Nagamine, Tsukuba, Ibaraki, 305-0052, Japan

15 ⁶ Deutsches Zentrum für Luft- und Raumfahrt (DLR), Institut für Physik der Atmosphäre, Oberpfaffenhofen, Germany

⁷ Atmospheric Chemistry Observations and Modeling Laboratory, National Center for Atmospheric Research, 3090 Center Green Drive, Boulder, CO, 80301, USA

⁸ Steinbuch Centre for Computing, Karlsruhe Institute of Technology, Karlsruhe, Germany

⁹ NASA Goddard Space Flight Center, Greenbelt, MD, USA

20 ¹⁰ Universities Space Research Association (USRA), GESTAR, Columbia, MD, USA

¹¹ National Center for Atmospheric Research, Boulder, CO, USA

¹² Global Monitoring Division, NOAA Earth System Research Laboratory, Boulder, CO,

* Now at: Climate and Space Sciences and Engineering, University of Michigan, Ann Arbor, MI 48109, USA

25

Correspondence to: Yuanhong Zhao (yuanhong.zhao@lsce.ipsl.fr) and Bo Zheng (bo.zheng@lsce.ipsl.fr)



Abstract

30 Decadal trends and interannual variations in the hydroxyl radical (OH), while poorly constrained at present, are critical for understanding the observed evolution of atmospheric methane (CH₄). Through analyzing the OH fields simulated by the model ensemble of the Chemistry-Climate Model Initiative (CCMI), we find (1) the negative OH anomalies during the El Niño years mainly corresponding to the enhanced carbon monoxide (CO) emissions from biomass burning and (2) a positive OH trend during
35 1980-2010 dominated by the elevated primary production and the reduced loss of OH due to decreasing CO after 2000. Both two-box model inversions and variational 4D inversions suggest that ignoring the negative anomaly of OH during the El Niño years leads to a large overestimation of the increase in global CH₄ emissions by up to 10Tg yr⁻¹ to match the observed CH₄ increase over these years. Not accounting for the increasing OH trends given by the CCMI models leads to an underestimation of the CH₄ emission
40 increase by ~23Tg yr⁻¹ from 1986 to 2010. The variational inversion estimated CH₄ emissions show that the tropical regions contribute most to the uncertainties related to OH. This study highlights the significant impact of climate and chemical feedbacks related to OH on the top-down estimates of the global CH₄ budget.



45 1 Introduction

Methane (CH_4) in the Earth's atmosphere is a major anthropogenic greenhouse gas that has resulted in a 0.62 W m^{-2} additional radiative forcing from 1750 to 2011 (Etminan et al., 2016). The tropospheric CH_4 mixing ratio has more than doubled between pre-industrial and the present day, which is unambiguously attributed to the increasing anthropogenic CH_4 emissions (Etheridge et al., 1998). Although the centennial and inter-decadal trends and the drivers of CH_4 growth are fairly clear, it is still challenging to understand the trends and the associated interannual variations on a time scale of 1-30 years. For example, the mysterious stagnation in CH_4 mixing ratios during 2000-2007 (Dlugokencky, NOAA/ESRL, 2019) is still under debate, highlighting the need for closing gaps in the global CH_4 budget on decadal time scales (e.g. Turner et al., 2019).

55 One of the barriers to understanding atmospheric CH_4 changes is the CH_4 sink, which is mainly the chemical reaction with the hydroxyl radical (OH) (Saunois et al., 2016; 2017; 2019; Zhao et al., 2020) that determines the tropospheric CH_4 lifetime. The burden of atmospheric OH is determined by complex and coupled atmospheric chemical cycles influenced by anthropogenic and natural emissions of multiple atmospheric reactive species, and also by climate change (Murray et al., 2013; Turner et al., 2018, Nicely et al., 2018), making it difficult to diagnose OH temporal changes from a single process. The OH source mainly include the primary production from the reaction of excited oxygen atoms ($\text{O}(^1\text{D})$) with water vapor (H_2O) and the secondary production mainly from the reaction of nitrogen oxide (NO) or ozone (O_3) with hydroperoxyl radical (HO_2) or organic peroxy radicals (RO_2). The OH sinks mainly include the reaction of OH with carbon monoxide (CO), CH_4 , or non-methane volatile organic compounds (NMVOCs).

65 Based on inversions of *1-1-1 trichloroethane* (methyl chloroform, MCF) atmospheric observations, some previous studies have attributed part of the observed CH_4 changes to the temporal variation in OH



70 concentrations ($[\text{OH}]$) but report large uncertainties in their estimates (McNorton et al 2016; Rigby et al. 2008, 2017; Turner et al., 2017). Such proxy approaches based on MCF inversions also have limitations in their accuracy, both due to uncertainties in MCF emissions before the 1990s, and the weakening of MCF gradients after the 1990s (Krol et al., 2003, Bousquet et al., 2005; Montzka et al., 2011; Prather and Holmes, 2017).

75 The OH variations have been explored with atmospheric chemistry models in terms of climate change (Nicely et al., 2018), anthropogenic emissions (Gaubert et al. 2017), and lightning NO_x emissions (Murray et al., 2013; Turner et al., 2018). The El Niño-Southern Oscillation (ENSO) has proven to influence $[\text{OH}]$ by perturbing CO emissions from biomass burning (Rowlinson et al. 2019) and NO_x emissions from
80 lightning (Turner et al., 2018), but the detailed mechanisms behind present OH variations and their impact on the CH_4 budget remain poorly understood. Nguyen et al. (2020) estimated the impact of the chemical feedback induced by CO and CH_4 changes on the top-down estimates of CH_4 emissions using a box model approach. However, they account neither for the heterogeneous distribution of atmospheric reactive species in space nor for the chemical feedback related to OH production processes that vary over time.
85 Understanding the influences of the chemical feedback related to OH on CH_4 emissions as estimated by atmospheric inversions is urgently needed and can benefit from better incorporating 3D simulations from atmospheric chemistry models.

Here we continue our former studies (Zhao et al., 2019; 2020), in which we have quantified the impact of
90 OH on top-down estimates of CH_4 emissions during the 2000s. This work aims to better understand the production and loss processes of OH and quantitatively assess their influence on the temporal changes of CH_4 lifetime and the global CH_4 budget on decadal-scale from 1980 to 2010. We first analyze the trends and year-to-year variations of nine independent OH fields covering the period of 1980-2010 simulated by the phase 1 of the International Global Atmospheric Chemistry (IGAC)/Stratosphere-troposphere



95 Processes and their Role in Climate (SPARC) Chemistry-Climate Model Initiative (CCMI) models
(Morgenstern et al., 2017) and then assess the contribution of different chemical processes to the OH
budget by estimating the main OH production and loss processes. We finally estimate the impact of OH
year-to-year variations and trends on the top-down estimation of global CH₄ emissions. Two-box model
inversions and the variational 4D inversions are both used to assess how the nonlinear chemical feedback
100 related to OH influences our understanding of the trends and drivers of the global CH₄ budget.

2 Method

2.1 CCMI OH fields

In this study, we analyze the OH fields simulated by five models (CESM1-CAM4Chem, CESM1-
105 WACCM, EMAC-L90MA, GEOSCCM, MRI-ESM1r1), which include detailed tropospheric ozone
chemistry and multiple primary VOC emissions. All five models conducted the REF-C1 experiments
(free-running simulations driven by state-of-the-art historical forcings including sea surface temperature
and sea ice concentrations) for 1960-2010, and four of them (excluding GEOSCCM) conducted the
REFC-1SD experiments (similar to REF-C1 but nudged to the reanalysis meteorology data) for 1980-
110 2010. Thus, we have nine OH fields generated by models with different chemistry, physics, and dynamics
covering the period 1980-2010. A detailed description of these CCMI models, experiments and
characteristics of the OH fields can be found in Morgenstern et al. (2017) and Zhao et al. (2019).

To eliminate the influence of different magnitudes of global OH burden simulated by those models, we
115 scale all OH fields to the same CH₄ loss for the year 2000 based on the reaction with OH used in the
TRANSCOM inter-comparison exercise (Patra et al., 2011). The inferred global mean scaling factors are
calculated for the year 2000 and for each OH field and then applied to the whole period. The production
(O(¹D)+H₂O, NO+HO₂, O₃+HO₂) and loss processes (removal of OH by CO, CH₄, formaldehyde (CH₂O),
and isoprene) for each OH field are estimated using the CCMI database (Section S1). For each OH fields,



120 we separate trends and year-to-year variations of the global tropospheric mean OH concentration
([OH]_{GM-CH₄}, [OH] weighted by reaction rate of OH with CH₄ multiplied by dry air mass, Lawrence et al.,
2001) as well as of its production and loss rates.

2.2 Atmospheric inversion systems

125 To evaluate the influences of OH temporal variations on the top-down estimation of CH₄ emissions, we
have conducted Bayesian atmospheric inversions using: 1) a two-box model similar to that described by
Turner et al. (2017) and 2) a 4D variational inversion system based on the version LMDz5B of the LMDz
atmospheric transport model under the PYVAR-SACS framework (Chevallier et al., 2007; Pison et al.,
2009) as described by Locatelli et al. (2015) and Zhao et al. (2020). The two-box model inversions allow
130 us to easily conduct multiple long-term global scale inversions (1984-2012) with each of the nine OH
fields to estimate the global CH₄ emission variations caused by various OH fields. The variational
inversions allow us to better represent the atmospheric transport and to address regional CH₄ emission
distributions. Thus, we have conducted both, two-box model inversions with each of the nine OH fields,
and variational inversions with the multi-model mean OH field (average of the nine OH fields).

135 Both the box model and the variational inversions optimize the CH₄ emissions and initial mixing ratios
by assimilating the observation data from the Earth System Research Laboratory of the US National
Oceanic and Atmospheric Administration (NOAA/ESRL, Dlugokencky et al. (1994)). The OH
concentrations are prescribed and not optimized in both inversion systems. A detailed description of the
140 two-box model, the LMDz atmospheric transport model, and the variational inversion method used here
are provided in the supplementary material (Section S2).

2.3 Ensemble of different inversions

We have designed an ensemble of inversion experiments as listed in Table 1 using the two-box model



145 with each OH field. Here, Inv_OH_std uses the aforementioned scaled OH fields; Inv_OH_cli uses a
climatology of each OH field, which is constant over the years and correspond to an average over 1980-
2010; Inv_OH_var stands for the detrended OH (only keeping the year-to-year variations); Inv_OH_trend
uses the OH without the year-to-year variability (retaining only the trend). By comparing Inv_OH_cli
with Inv_OH_std, Inv_OH_var, and Inv_OH_trend, it is possible to assess the influence of total OH
150 temporal changes, year-to-year variations, and OH trends on the overall CH₄ changes, respectively. The
box model inversions are conducted from 1984 to 2012 (2010 OH fields are used for 2011 and 2012). The
first and last two years are treated as spin-up and spin-down, and we only analyze the inversion results
over 1986-2010.

155 We have conducted two variational inversions, Inv_OH_std and Inv_OH_cli, using the multi-model mean
OH field to test the influence of OH temporal variations on the top-down estimates of global to regional
CH₄ emissions. The LMDz inversions are conducted for four time periods (1994-1997, 1996-1999, 2000-
2004, and 2006-2010; first and last years as spin-up and spin-down; Sect.3.4). The four time periods are
chosen to represent the transition from La Niña (1995-1996) to El Niño (1997-1998) years and the years
160 of stagnated (2001-2003) and renewed growth (2007-2009) of observed CH₄.

3 Results

3.1 Decadal OH trends and year-to-year variability

All CCMI models simulate positive OH trends from 1980 to 2010 after removing the year-to-year
165 variability (Fig.1, top panel), consistent with previous analyses of CCMI OH fields (Zhao et al., 2019;
Nicely et al., 2020) and model results of the Aerosol and Chemistry Model Intercomparison Project
(Stevenson et al., 2020). The multi-model mean [OH]_{GM-CH₄} increased by $0.7 \times 10^5 \text{ molec cm}^{-3}$ from 1980
to 2010. The growth rates in [OH]_{GM-CH₄} are estimated as $\sim 0.03 \times 10^5 \text{ molec cm}^{-3} \text{ yr}^{-1}$ ($0.3\% \text{ yr}^{-1}$) during

the early 1980s, $\sim 0.01 \times 10^5 \text{ molec cm}^{-3} \text{ yr}^{-1}$ (0.1% yr^{-1}) between the mid-1980s and the late-1990s, and
170 $0.03\text{-}0.05 \times 10^5 \text{ molec cm}^{-3} \text{ yr}^{-1}$ (0.3%-0.5% yr^{-1}) since the 2000s. This continuously increases in [OH] is
different from the results based on the MCF inversions using the two-box model approach (Turner et al.,
2017; Rigby et al., 2017), which yield increases in [OH] from the 1990s to the early 2000s and a decreases
in OH afterward.

175 The ensemble of the anomaly of detrended $[\text{OH}]_{\text{GM-CH}_4}$ (middle panel of Fig.1) shows a strong anti-
correlation ($r = -0.50$) with the bi-monthly Multivariate ENSO Index Version 2 (MEI, the bottom panel
of Fig.1 and Section S3) (Zhang et al., 2019), with higher $[\text{OH}]_{\text{GM-CH}_4}$ during La Niña and lower $[\text{OH}]_{\text{GM-CH}_4}$
during El Niño. From 1980 to 2010, the CCMi model simulations show several negative $[\text{OH}]_{\text{GM-CH}_4}$
anomalies, the three largest reaching as high as $-0.36 \pm 0.23 \times 10^5 \text{ molec cm}^{-3}$ ($-3.5 \pm 2.2\%$) during 1982-
180 1983, $-0.37 \pm 0.17 \times 10^5 \text{ molec cm}^{-3}$ ($-3.6 \pm 1.7\%$) during 1991-1992, and $-0.49 \pm 0.37 \times 10^5 \text{ molec cm}^{-3}$ ($-$
 $4.7 \pm 3.5\%$) during 1997-1998. The negative $[\text{OH}]_{\text{GM-CH}_4}$ anomalies during 1982-1983 and 1997-1998
correspond to the two strongest El Niño events ($\text{MEI} > 2.5$). During 1991-1992, the negative $[\text{OH}]_{\text{GM-CH}_4}$
anomaly corresponds to both, the weaker El Niño event (MEI up to 2.0), and the eruption of Mount
Pinatubo. During other weak El Niño events (1986-1987, 2002-2003, 2004-2005, and 2006-2007), the
185 multi-model mean $[\text{OH}]_{\text{GM-CH}_4}$ shows smaller negative anomalies of 1-2%. Only the negative OH
anomaly during 2006-2007 ($2.2 \pm 1.0\%$) is simulated by all models. The negative anomalies are consistent
with an up to 9% reduction of [OH] during 1997-1998 simulated by TOMCAT-GLOMAP as shown by
Rowlinson et al. (2019), as well as a 5% reduction of [OH] over tropical regions during 1991-1993
constrained by MCF observations (Bousquet et al, 2006). During La Niña events, the $[\text{OH}]_{\text{GM-CH}_4}$ shows
190 $\sim 2\%$ positive anomalies, resulting in more than a 6% increase in OH ($\text{max} - \text{min}$) during 1983-1985,
1992-1994, and 1998-2000.

The negative $[\text{OH}]_{\text{GM-CH}_4}$ anomalies during strong El Niño events correspond to the highest growth rates



of the CH₄ mixing ratio from the surface observations (*Dlugokencky, NOAA/ESRL*), which are
195 14.0±0.6ppbv yr⁻¹ in 1991, and 12.1±0.8ppbv yr⁻¹ in 1998 (Fig.S1). The positive anomalies of [OH]<sub>GM-
CH₄</sub> during La Niña events correspond to a much smaller CH₄ growth (e.g. 3.8±0.6ppbv yr⁻¹ in 1993 and
2.3±0.8ppbv yr⁻¹ in 1999) (Fig. S1).

3.2 Factors controlling OH trends and year-to-year variability

200 The changes in tropospheric [OH] are due to changes in the balance of production and loss processes.
Here we assess the drivers of OH year-to-year variations and trend by calculating the OH production and
loss processes listed in Table 2 following Murray et al. (2013; 2014). The multi-model calculated OH
production/loss in the troposphere averaged over 1980-2010 is 209.3±11.9Tmol yr⁻¹, similar to that
~200Tmol yr⁻¹ reported by Murray et al. (2014). Of the total OH production, 46% (96.2±1.9Tg yr⁻¹) are
205 from primary production (O(¹D) +H₂O). Two main secondary productions, NO+NO₂, and O₃+HO₂
account for 30% (62.6±4.1Tmol yr⁻¹) and 13% (26.2±1.9Tmol yr⁻¹), respectively. For the OH loss,
reactions with CO and CH₄ account for 39% (82.3±3.8Tmol yr⁻¹) and 15% (32.4±1.4Tmol yr⁻¹),
respectively. We have also calculated the OH loss by reactions with isoprene (C₅H₈) and formaldehyde
(CH₂O), which both remove 6% of OH, reflecting the influences of NMVOCs from natural and
210 anthropogenic sources, respectively. Besides, there are 12% of OH production and 33% of OH loss not
analyzed here due to lack of data in the CCM1 model outputs (e.g. OH loss due to reaction with NMVOCs
included in difference models).

Fig.2 shows the changes in the trends of OH production and loss processes (year-to-year variations are
215 removed) with respect to the year 1980. The OH primary production (O(¹D)+H₂O) shows a large increase
of 10.1±1.1Tmol yr⁻¹ from 1980 to 2010, as the dominant driver of the positive OH trend. The increase
in OH primary production is due to an increase in both tropospheric O₃ burden (producing O(¹D)) and
water vapor (Zhao et al., 2019; Nicely et al., 2020). The OH loss from CO increased by 7.3±0.7Tmol yr⁻¹



220 ¹ from 1980 to 2001 but then decreased by $4.2 \pm 2.2 \text{ Tmol yr}^{-1}$ from 2001 to 2010. We find that the decrease
in OH loss by CO can explain the accelerated OH increase after 2000, despite a stagnated OH primary
production and a slight decrease of the OH secondary production. The OH loss by CH₄, which shows a
continuous increase of $6.2 \pm 0.5 \text{ Tmol yr}^{-1}$ from 1980 to 2010, buffers the increase in OH production by NO
($5.3 \pm 1.1 \text{ Tmol yr}^{-1}$). The OH production by O₃+HO₂, as well as OH loss by CH₂O and isoprene, show
smaller changes of $2.1 \pm 1.1 \text{ Tmol yr}^{-1}$, $1.9 \pm 0.3 \text{ Tmol yr}^{-1}$, and $1.1 \pm 0.6 \text{ Tmol yr}^{-1}$, respectively, during 1980-
225 2010. By comparing the magnitude of the production and loss processes, we conclude that an enhanced
OH primary production and changes in OH loss by CO are the most important factors leading to the
increased OH trend inferred by CCMI models from 1980 to 2010.

230 Fig.3 and Fig.S2 show the year-to-year variations of the global total OH production and loss due to several
processes (calculated after trends have been removed). Year-to-year variations of global [OH] are mainly
determined by the primary (O(¹D)+H₂O) and secondary production (NO+HO₂; O₃+HO₂) and by OH loss
due to CO (Fig.3). Other OH loss processes, including reactions with CH₄, CH₂O, and isoprene, show
much smaller year-to-year variations but larger uncertainties (Fig.S2), revealing a larger model spread for
these processes.

235 As shown in Fig.3, negative anomalies of [OH] during El Niño events are dominated by increased OH
loss through the reaction with CO in response to enhanced biomass burning (Fig.S3), similar to the
conclusions of Rowlinson et al. (2019) and Nicely et al. (2020). During the strong El Niño events in 1982-
1983, 1991-1992, and 1997-1998, the OH loss by CO increased by up to $3.4 \pm 0.4 \text{ Tmol yr}^{-1}$, $4.5 \pm 0.6 \text{ Tmol}$
240 yr^{-1} , and $7.6 \pm 0.5 \text{ Tmol yr}^{-1}$, respectively, compared to the mean value of 1980-2010. The increase of OH
loss by CO can be partly offset by an increase in OH production. Indeed, in 1998, the OH primary
production (O(¹D)+H₂O), OH produced by NO+RO₂, and O₃+RO₂ increased by $3.2 \pm 0.7 \text{ Tmol yr}^{-1}$,
 $2.7 \pm 0.5 \text{ Tmol yr}^{-1}$, and $1.6 \pm 0.3 \text{ Tmol yr}^{-1}$, respectively, offsetting most of the OH loss increase. The



increase in OH primary production is mainly due to an increase in tropospheric water vapor and O₃ burden
245 during El Niño events (Fig.S3 and S12 in Nicely et al. (2020)), while the increase in OH secondary
production is caused by enhanced NO_x emissions (Fig.S3) and O₃ formation (Nicely et al. (2020) related
to biomass burning as well as more HO₂ formation by CO+OH. As a result, the OH year-to-year variations
found here are much smaller than those estimated by Nguyen et al. (2020), who mainly considered the
response of OH to CO. The positive anomaly OH primary production ($0.2 \pm 0.5 \text{ Tmol yr}^{-1}$) is not significant
250 during 1991-1992 El Niño event, maybe due to reduction of tropospheric water vapor (Fig.S3 in Nicely
et al. (2020)) after the eruption of Mount Pinatubo (Soden et al., 2020). Thus, the negative [OH] anomaly
during the weak El Niño event in 1991-1992 is potentially being enhanced by the eruption of Mount
Pinatubo. Previous studies have shown that NO_x emissions from lightning can contribute to the OH
interannual variability (Murray et al., 2013; Turner et al. 2018). In addition, soil NO_x emissions depend
255 on temperature and soil humidity (Yienger and Levy, 1995), which vary during the El Niño events. The
year-to-year variations of NO_x emissions from lightning show large differences among CCM1 models
(Fig. S4), and only EMAC and GEOSCCM apply interactive soil NO_x emissions that vary with
meteorology conditions (Morgenstern et al., 2017) based on Yienger and Levy (1995). Thus NO_x
emissions from lightning and soil mainly contribute to inter-model differences instead of showing a
260 consistent response to El Niño.

Using a machine learning method, Nicely et al. (2020) attributed the positive [OH] trend simulated by the
CCMI models mainly to the increase of tropospheric O₃, J(O¹D), NO_x and H₂O, and attributed [OH]
interannual variations to CO changes. Overall, the explanations of the drivers of OH year-to-year
265 variations and trends found in our process analysis are broadly consistent with those reported by Nicely
et al. (2020), and we emphasize that the decrease of CO emission and concentrations after 2000 (Zheng
et al., 2019) is important for determining the accelerated positive OH trend.



3.3 Impact of OH variation on the top-down estimation of CH₄ budget

270 Fig.4a shows the anomaly of global total CH₄ emission estimated by inv_OH_std (nine scaled OH fields;
yellow line) and inv_OH_cli (nine climatological OH; blue line) using the two-box model during 1986-
2010. With the climatological OH fields (blue line), the top-down estimated CH₄ emissions show no clear
trend before 2005, with large positive anomalies during strong El Niño years. There are two peaks of
positive CH₄ emission anomalies during this period, 10.0Tg yr⁻¹ in 1991, and 14.4Tg yr⁻¹ in 1998. From
275 2005 to 2008, the CH₄ emissions show a large increase of 26.1Tg yr⁻¹.

The OH temporal variations are found to largely influence the interannual changes of top-down estimated
CH₄ emissions (yellow line of Fig. 4a), with differences between the two inversions reaching up to more
than 15Tg yr⁻¹ (Fig.4b). The contribution from the OH year-to-year variations and trends are also shown
280 in Fig.4. The negative anomalies of OH during El Niño years reduce the unusually high top-down
estimated CH₄ emissions in 1991-1992 by 6.7 ± 2.6 Tg yr⁻¹, and in 1998 by 9.7 ± 3.1 Tg yr⁻¹ (Fig.4c). As a
result, the high emission peaks to match the observed CH₄ mixing ratio growth in 1991 (14.2ppb yr⁻¹) and
1998 (12.1ppbv yr⁻¹), as estimated using the climatological OH are largely reduced.

285 The identified positive OH trend leads to an additional 23.2 ± 8.7 Tg yr⁻¹ increase in CH₄ emissions from
1986 to 2010 (Fig.4d). During 1986-2005, the mean CH₄ emissions, as estimated with the scaled OH,
show a positive trend of 0.63 ± 0.43 Tg yr⁻² ($P < 0.05$). For 1986-2005, increased CH₄ emissions offset the
increase in the OH sink to match the observations. From 2005 to 2008, in contrast to previous studies,
which attribute the increased observed CH₄ mixing ratios to decreased OH based on MCF inversions
290 (Turner et al., 2017, Rigby et al., 2017), the increasing OH trend simulated by CCMI models results in an
additional 4.9 ± 1.6 Tg yr⁻¹ CH₄ emission increase in the inversion to match the observations.

We compare the inversion using the two-box model (“X” in Fig.5) with the results from the variational



approach (bars in Fig.5), using the multi-model mean OH field, to evaluate the performance of the
295 simplified two-box model inversions. Despite the limitations inherent to two-box model inversions, such
as treatment of inter-hemispheric transport, stratospheric loss, and the impact of spatial variability (Naus
et al., 2019), the two-box model inversion estimates similar temporal changes of CH₄ emissions and losses
compare to the variational approach for the four periods (Fig.5, left and middle), as well as their response
to OH changes (Fig.5, right), on a global scale. Such comparisons reinforce the reliability of the
300 conclusions made from the two-box model inversions regarding changes in the global total CH₄ budget.

The variational inversions allow us to access the regional contribution of the drivers to observed
atmospheric CH₄ mixing ratio changes. Here, as a synthesis, we focus on four latitude bands (Fig.5 and
Table S2), including the southern extra-tropical regions (90 °S-30 °S), the tropical regions (30 °S-30 °N),
305 and the northern temperate (30 °-60 °N) and boreal (60 °-90 °N) regions. On average, OH over the tropical
and northern temperate regions removes 74% and 14% of global total atmospheric CH₄, respectively.

Between the periods 1995-1996 and 1997-1998, if one does not consider the OH temporal variations
(Inv_OH_cli), the CH₄ loss by OH shows a slight increase of 1.9Tg yr⁻¹ due to an increase of atmospheric
310 CH₄ mixing ratios. The main driver of observed atmospheric CH₄ mixing ratio changes is the 9.5Tg yr⁻¹
increase of CH₄ emission over tropics and the 6.8Tg yr⁻¹ increase over the northern temperate regions
(middle panel of Fig.5 and Table S2). When the multi-model mean OH temporal variations are included
(Inv_OH_std), the negative anomaly of OH in 1997-1998 led to a 9.4Tg yr⁻¹ decrease in CH₄ loss in 1997-
1998 compared to 1995-1996, of which 7.4Tg yr⁻¹ (78%) are contributed by the tropical regions (left panel
315 of Fig.5). As a result, the decrease of CH₄ loss by OH contributes a bit more to match the observed CH₄
mixing ratios increase during the El Niño periods than the changes in CH₄ emissions (a global increase
of 8.2Tg yr⁻¹). The emission increases from 1995-1996 to 1997-1998 over the tropics and the northern
temperate regions are reduced to 2.7Tg yr⁻¹ and 4.8Tg yr⁻¹ (left panel of Fig.5, Inv_OH_std), respectively,



similar to the inversion results given by Bousquet et al. (2006).

320

From the period 2001-2003 to 2007-2009, positive OH trends lead to a 13.0Tg yr^{-1} increase of the CH_4 loss, of which 9.9Tg yr^{-1} (76%) originates from the tropics (Inv_OH_std, left panel of Fig.5). In response to increased CH_4 losses, the increase of optimized emissions over tropical regions (15.7Tg yr^{-1} , Inv_OH_std) is more than twice of the inversion using climatological OH (7.3Tg yr^{-1} , Inv_OH_cli). The emission increases during the two periods over the northern region show a smaller change of 2.0Tg yr^{-1} (12.3Tg yr^{-1} estimated by Inv_OH_std versus 10.3Tg yr^{-1} by Inv_OH_cli, Fig. 5). The variational inversions show that the OH temporal variations are most critical for top-down estimates of CH_4 budgets over the tropical regions since OH over tropical regions shows larger interannual variations and trend than mid to high latitude regions (Fig.S5) and most of the CH_4 (74%) is removed from the atmosphere by OH over the tropical regions.

330

4 Conclusion and discussion

Based on the simulations from the CCMI, we explore the response of OH fields to changes in climate, anthropogenic and natural emissions and its impact on the top-down estimates of CH_4 emissions during 1980-2010 based on a model perspective. We find that although CCMI models simulated rather different global total burdens of OH (Zhao et al., 2019), they show very similar patterns in temporal variations, including (1) negative anomalies during El Niño years, which are mainly driven by an elevated OH loss by reaction with CO from enhanced biomass burning, despite a partial buffering through enhanced OH production, and (2) a continuously increasing in OH from 1980, which is mostly contributed by OH primary production and accelerating after 2000 due to reduced CO emissions. By conducting inversions using a two-box model and a variational approach together with the ensemble of CCMI OH fields, we find that (1) the OH year-to-year variations can largely reduce the CH_4 emission increase (by up to 10Tg yr^{-1}) needed to match the observed CH_4 increase during El Niño years, and (2) the positive OH trend

340



345 results in $23.2 \pm 8.7 \text{ Tg yr}^{-1}$ additional increase in optimized emissions from 1986 to 2010 compared to the
inversions using constant OH. The variational inversions also show that OH temporal variations mainly
influence top-down estimates of CH_4 emissions over tropical regions.

The responses of OH to changes in biomass burning, ozone, water vapor, and lightning NO_x emissions
during El Niño years have been recognized by previous studies (Holmes et al., 2013; Murray et al., 2014;
350 Turner et al., 2018; Rowlinson et al., 2019; Nguyen et al., 2020). Here, the consistent temporal variations
of CCMI OH fields increase our confidence in the model simulated response of OH to ENSO as a result
of several nonlinear chemical processes. One of the largest uncertainties is NO_x emissions from lightning,
which have been proven to contribute to year-to-year variations in OH (Murray et al., 2013; Turner et al.,
2018), but here show a large spread among CCMI models. In addition, NO_x emissions from soil may also
355 change during El Niño years. Improving estimates of NO_x emissions from lightning based on satellite
observations (Murray et al., 2013) and a better representation of the interactive NO_x emissions from the
soil are critical for improving the model simulation of OH temporal variability and for top-down estimates
of year-to-year variations of CH_4 emissions.

360 The positive trend of OH after the mid-2000s, which results in enhanced top-down estimated CH_4
emissions over the tropics, is opposite to those constrained by MCF inversions (Turner et al., 2017; Rigby
et al., 2017). However, the processes that control the model simulated positive OH trend are supported by
current studies based on observations, including decreased CO emissions (Zheng et al., 2019), small
variations of global NO_x emissions (Miyazaki et al., 2017), and an increase in tropospheric ozone (Ziemke
365 et al., 2019) and water vapor (Chung et al., 2014). Given the large uncertainty existing in MCF-
constrained OH (Krol et al., 2003, Bousquet et al., 2005; Montzka et al., 2011; Prather and Holmes, 2017;
Naus et al. et al., 2019) and the evidence for increasing OH given by CCMI models and other literature,
the accuracy of MCF-based OH inversions after the mid-2000s remains an open problem and the large

370 discrepancy between MCF-based and CCMI model simulated OH trends requires more effort to close the
gap.

The temporal variations of OH are generally less considered in current top-down estimates of CH₄
emissions, implying potential additional uncertainties in the global CH₄ budget (Saunois et al., 2017;
Zhao et al., 2020). The tropical regions, where top-down estimated CH₄ emissions show the largest
375 sensitivity to OH changes, represent more than 60% of CH₄ emissions worldwide (Saunois et al., 2016).
The tropical CH₄ emissions are dominated by wetland emissions, of which large uncertainties exist in
both bottom-up and top-down studies (Saunois et al., 2016; 2017). The variational inversions using OH
with temporal variations attribute the observed rising CH₄ growth during El Niño to the reduction of CH₄
loss instead of enhanced emissions over tropics, which are consistent with process-based wetland models
380 that estimated wetland CH₄ emission reductions at beginning of El Niño event (Hodson et al., 2011; Zhang
et al., 2018). Future climate projections show that the extreme El Niño events will be more frequent under
a warmer climate (Rao et al., 2019), which may enhance the fluctuations in [OH]. Furthermore, the
changes in anthropogenic emissions, e.g. such as expected decreases in NO_x emissions (Lamarque et al.,
2013), can also affect the OH trends. Our research highlights the importance of considering climate
385 changes and chemical feedbacks in future CH₄ budget research.

Data availability

The CCMI OH fields are available at the Centre for Environmental Data Analysis
(CEDA; <http://data.ceda.ac.uk/badc/wcrp-ccmi/data/CCMI-1/output>; Hegglin and Lamarque, 2015), the
390 Natural Environment Research Council's Data Repository for Atmospheric Science and Earth
Observation. The CESM1-WACCM outputs for CCMI are available
at <http://www.earthsystemgrid.org> (Climate Data Gateway at NCAR, 2019). The surface observations for
CH₄ inversions are available at the World Data Centre for Greenhouse Gases (WDCGG,
<https://gaw.kishou.go.jp/>, 2019). Other datasets can be accessed by contacting the corresponding author.

395



Author contributions

YZ, BZ, MS, and PB designed the study, analyzed data and wrote the manuscript. AB developed the LMDz code for variational CH₄ inversions. ED provided the atmospheric in situ data. MH, MD, PJ, DK, 400 OK, SS, and ST provided CCM1 model outputs. All co-authors commented on the manuscript.

Acknowledgements

This work benefited from the expertise of the Global Carbon Project methane initiative.

We acknowledge the modeling groups for making their simulations available for this analysis, the joint 405 WCRP SPARC/IGAC Chemistry–Climate Model Initiative (CCMI) for organizing and coordinating the model simulations and data analysis activity, and the British Atmospheric Data Centre (BADC) for collecting and archiving the CCM1 model output.

The EMAC model simulations have been performed at the German Climate Computing Centre (DKRZ) through support from the Bundesministerium für Bildung und Forschung (BMBF). DKRZ and its 410 scientific steering committee are gratefully acknowledged for providing the HPC and data archiving resources for the consortial project ESCiMo (Earth System Chemistry integrated Modelling).

Makoto Deushi was partly supported by JSPS KAKENHI grant no. JP19K12312.

Yuanhong Zhao acknowledges helpful discussions with Zhen Zhang, Yilong Wang, and Lin Zhang.

Competing interests

415 The authors declare that they have no conflicts of interest.

Financial support

This research has been supported by the Gordon and Betty Moore Foundation (grant no. GBMF5439), “Advancing Understanding of the Global Methane Cycle”.

420 Reference

Bousquet, P., Hauglustaine, D. A., Peylin, P., Carouge, C., and Ciais, P.: Two decades of OH variability as inferred by an inversion of atmospheric transport and chemistry of methyl chloroform, *Atmos. Chem. Phys.*, 5, 2635-2656, 10.5194/acp-5-2635-2005, 2005.



- 425 Bousquet, P., Ciais, P., Miller, J. B., Dlugokencky, E. J., Hauglustaine, D. A., Prigent, C., Van der Werf, G. R., Peylin, P., Brunke, E. G., Carouge, C., Langenfelds, R. L., Lathiere, J., Papa, F., Ramonet, M., Schmidt, M., Steele, L. P., Tyler, S. C., and White, J.: Contribution of anthropogenic and natural sources to atmospheric methane variability, *Nature*, 443, 439-443, 10.1038/nature05132, 2006.
- Chevallier, F., Br éon, F.-M., and Rayner, P. J.: Contribution of the Orbiting Carbon Observatory to the estimation of CO₂ sources and sinks: Theoretical study in a variational data assimilation framework, *Journal of Geophysical Research: Atmospheres*, 112, 10.1029/2006jd007375, 2007.
- 430 Chung, E.-S., Soden, B., Sohn, B. J., and Shi, L.: Upper-tropospheric moistening in response to anthropogenic warming, *Proceedings of the National Academy of Sciences*, 111, 11636-11641, 10.1073/pnas.1409659111, 2014.
- Dlugokencky, E., Steele, L., Lang, P., and Masarie, K.: The growth rate and distribution of atmospheric methane, *Journal of Geophysical Research: Atmospheres*, 99, 17021-17043, 1994.
- 435 Dlugokencky, NOAA/ESRL ,www.esrl.noaa.gov/gmd/ccgg/trends_ch4/, 2020
- Etheridge, D. M., Steele, L. P., Francey, R. J., and Langenfelds, R. L.: Atmospheric methane between 1000 A.D. and present: Evidence of anthropogenic emissions and climatic variability, *Journal of Geophysical Research: Atmospheres*, 103, 15979-15993, 10.1029/98jd00923, 1998.
- 440 Etminan, M., Myhre, G., Highwood, E. J., and Shine, K. P.: Radiative forcing of carbon dioxide, methane, and nitrous oxide: A significant revision of the methane radiative forcing, *Geophysical Research Letters*, 43, 12,614-612,623, doi:10.1002/2016GL071930, 2016.
- Gaubert, B., Worden, H. M., Arellano, A. F. J., Emmons, L. K., Tilmes, S., Barr é J., Martinez Alonso, S., Vitt, F., Anderson, J. L., Alkemade, F., Houweling, S., and Edwards, D. P.: Chemical Feedback From Decreasing Carbon Monoxide Emissions, *Geophysical Research Letters*, 44, 9985-9995, 10.1002/2017gl074987, 2017.
- 445 Hegglin, M. I. and Lamarque, J.-F.: The IGAC/SPARC Chemistry-Climate Model Initiative Phase-1 (CCMI-1) model data output, NCAS British Atmospheric Data Centre, [ADD ACCESS DATE], available at: <http://catalogue.ceda.ac.uk/uuid/9cc6b94df0f4469d8066d69b5df879d5>, 2015.
- 450 Hodson, E. L., Poulter, B., Zimmermann, N. E., Prigent, C., and Kaplan, J. O.: The El Ni ño–Southern Oscillation and wetland methane interannual variability, *Geophysical Research Letters*, 38, 10.1029/2011gl046861, 2011.
- Holmes, C. D., Prather, M. J., S øvde, O. A., and Myhre, G.: Future methane, hydroxyl, and their uncertainties: key climate and emission parameters for future predictions, *Atmospheric Chemistry and Physics*, 13, 285-302, 10.5194/acp-13-285-2013, 2013.
- 455 Krol, M. C., Lelieveld, J., Oram, D. E., Sturrock, G. A., Penkett, S. A., Brenninkmeijer, C. A. M., Gros, V., Williams, J., and Scheeren, H. A.: Continuing emissions of methyl chloroform from Europe, *Nature*, 421, 131-135, 10.1038/nature01311, 2003.
- Lamarque, J. F., Shindell, D. T., Josse, B., Young, P. J., Cionni, I., Eyring, V., Bergmann, D., Cameron-Smith, P., Collins, W. J., Doherty, R., Dalsoren, S., Faluvegi, G., Folberth, G., Ghan, S. J., Horowitz, L.
- 460



- 465 W., Lee, Y. H., MacKenzie, I. A., Nagashima, T., Naik, V., Plummer, D., Righi, M., Rumbold, S. T.,
Schulz, M., Skeie, R. B., Stevenson, D. S., Strode, S., Sudo, K., Szopa, S., Voulgarakis, A., and Zeng, G.:
The Atmospheric Chemistry and Climate Model Intercomparison Project (ACCMIP): overview and
description of models, simulations and climate diagnostics, *Geoscientific Model Development*, 6, 179-
206, 10.5194/gmd-6-179-2013, 2013.
- Lawrence, M. G., Jöckel, P., and von Kuhlmann, R.: What does the global mean OH concentration tell
us?, *Atmos. Chem. Phys.*, 1, 37-49, 10.5194/acp-1-37-2001, 2001.
- 470 Locatelli, R., Bousquet, P., Hourdin, F., Saunois, M., Cozic, A., Couvreux, F., Grandpeix, J. Y., Lefebvre,
M. P., Rio, C., Bergamaschi, P., Chambers, S. D., Karstens, U., Kazan, V., van der Laan, S., Meijer, H. A.
J., Moncrieff, J., Ramonet, M., Scheeren, H. A., Schlosser, C., Schmidt, M., Vermeulen, A., and Williams,
A. G.: Atmospheric transport and chemistry of trace gases in LMDz5B: evaluation and implications for
inverse modelling, *Geosci. Model Dev.*, 8, 129-150, 10.5194/gmd-8-129-2015, 2015.
- 475 McNorton, J., Chipperfield, M. P., Gloor, M., Wilson, C., Feng, W., Hayman, G. D., Rigby, M., Krummel,
P. B., and Doherty, S., Prinn, R. G., Weiss, R. F., Young, D., Dlugokencky, E., and Montzka, S. A.:
Role of OH variability in the stalling of the global atmospheric CH₄ growth rate
from 1999 to 2006, *Atmospheric Chemistry and Physics*, 16, 7943-7956, 10.5194/acp-16-7943-2016,
2016.
- 480 Miyazaki, K., Eskes, H., Sudo, K., Boersma, K. F., Bowman, K., and Kanaya, Y.: Decadal changes in
global surface NO_x emissions from multi-constituent satellite data assimilation, *Atmos. Chem. Phys.*, 17,
807-837, 10.5194/acp-17-807-2017, 2017.
- Montzka, S. A., Krol, M., Dlugokencky, E., Hall, B., Jöckel, P., and Lelieveld, J.: Small Interannual
Variability of Global Atmospheric Hydroxyl, *Science*, 331, 67-69, 10.1126/science.1197640, 2011.
- 485 Morgenstern, O., Hegglin, M. I., Rozanov, E., and Connor, F. M., Abraham, N. L., Akiyoshi, H.,
Archibald, A. T., Bekki, S., Butchart, N., Chipperfield, M. P., Deushi, M., Dhomse, S. S., Garcia, R. R.,
Hardiman, S. C., Horowitz, L. W., Jöckel, P., Josse, B., Kinnison, D., Lin, M., Mancini, E., Manyin, M.
E., Marchand, M., Maréchal, V., Michou, M., Oman, L. D., Pitari, G., Plummer, D. A., Revell, L. E., Saint-
Martin, D., Schofield, R., Stenke, A., Stone, K., Sudo, K., Tanaka, T. Y., Tilmes, S., Yamashita, Y.,
Yoshida, K., and Zeng, G.: Review of the global models used within phase 1 of the Chemistry–Climate
Model Initiative (CCMI), *Geoscientific Model Development*, 10, 639-671, 10.5194/gmd-10-639-2017,
490 2017.
- Multivariate ENSO Index Version 2, available at <https://www.esrl.noaa.gov/psd/enso/mei/>, 2020
- Murray, L. T., Logan, J. A., and Jacob, D. J.: Interannual variability in tropical tropospheric ozone and
OH: The role of lightning, *Journal of Geophysical Research: Atmospheres*, 118, 4114-4148, 10.1002/jgrd.50857, 2013.
- 495 Murray, L. T., Mickley, L. J., Kaplan, J. O., Sofen, E. D., Pfeiffer, M., and Alexander, B.: Factors
controlling variability in the oxidative capacity of the troposphere since the Last Glacial Maximum,
Atmospheric Chemistry and Physics, 14, 3589-3622, 10.5194/acp-14-3589-2014, 2014.



- 500 Naus, S., Montzka, S. A., Pandey, S., Basu, S., Dlugokencky, E. J., and Krol, M.: Constraints and biases in a tropospheric two-box model of OH, *Atmos. Chem. Phys.*, 19, 407-424, 10.5194/acp-19-407-2019, 2019.
- Nguyen, N. H., Turner, A. J., Yin, Y., Prather, M. J., and Frankenberg, C.: Effects of Chemical Feedbacks on Decadal Methane Emissions Estimates, *Geophysical Research Letters*, 47, e2019GL085706, 10.1029/2019gl085706, 2020.
- 505 Nicely, J. M., Canty, T. P., Manyin, M., Oman, L. D., Salawitch, R. J., Steenrod, S. D., Strahan, S. E., and Strode, S. A.: Changes in Global Tropospheric OH Expected as a Result of Climate Change Over the Last Several Decades, *Journal of Geophysical Research: Atmospheres*, 123, 10,774-710,795, doi:10.1029/2018JD028388, 2018.
- Nicely, J. M., Duncan, B. N., Hanisco, T. F., Wolfe, G. M., Salawitch, R. J., Deushi, M., Haslerud, A. S., Jöckel, P., Josse, B., Kinnison, D. E., Klekociuk, A., Manyin, M. E., Maréchal, V., Morgenstern, O., Murray, L. T., Myhre, G., Oman, L. D., Pitari, G., Pozzer, A., Quaglia, I., Revell, L. E., Rozanov, E., Stenke, A., 510 Stone, K., Strahan, S., Tilmes, S., Tost, H., Westervelt, D. M., and Zeng, G.: A machine learning examination of hydroxyl radical differences among model simulations for CCM1-1, *Atmos. Chem. Phys.*, 20, 1341-1361, 10.5194/acp-20-1341-2020, 2020.
- Soden, B. J., Wetherald, R. T., Stenchikov, G. L., and Robock, A.: Global Cooling After the Eruption of 515 Mount Pinatubo: A Test of Climate Feedback by Water Vapor, *Science*, 296, 727-730, 10.1126/science.296.5568.727, 2002.
- Stevenson, D. S., Zhao, A., Naik, V., O'Connor, F. M., Tilmes, S., Zeng, G., Murray, L. T., Collins, W. J., Griffiths, P., Shim, S., Horowitz, L. W., Sentman, L., and Emmons, L.: Trends in global tropospheric hydroxyl radical and methane lifetime since 1850 from AerChemMIP, *Atmos. Chem. Phys. Discuss.*, 520 2020, 1-25, 10.5194/acp-2019-1219, 2020.
- Patra, P. K., Houweling, S., Krol, M., Bousquet, P., Belikov, D., Bergmann, D., Bian, H., Cameron-Smith, P., Chipperfield, M. P., Corbin, K., Fortems-Cheiney, A., Fraser, A., Gloor, E., Hess, P., Ito, A., Kawa, S. R., Law, R. M., Loh, Z., Maksyutov, S., Meng, L., Palmer, P. I., Prinn, R. G., Rigby, M., Saito, R., and 525 Wilson, C.: TransCom model simulations of CH₄ and related species: linking transport, surface flux and chemical loss with CH₄ variability in the troposphere and lower stratosphere, *Atmospheric Chemistry and Physics*, 11, 12813-12837, 10.5194/acp-11-12813-2011, 2011.
- Pison, I., Bousquet, P., Chevallier, F., Szopa, S., and Hauglustaine, D.: Multi-species inversion of CH₄, CO and H₂ emissions from surface measurements, *Atmos. Chem. Phys.*, 9, 5281-5297, 10.5194/acp-9-5281-2009, 2009.
- 530 Prather, M. J., and Holmes, C. D.: Overexplaining or underexplaining methane's role in climate change, *Proceedings of the National Academy of Sciences*, 114, 5324-5326, 10.1073/pnas.1704884114, 2017.
- Rao, V. B., Maneesha, K., Sravya, P., Franchito, S. H., Dasari, H., and Gan, M. A.: Future increase in extreme El Nino events under greenhouse warming increases Zika virus incidence in South America, *npj Climate and Atmospheric Science*, 2, 4, 10.1038/s41612-019-0061-0, 2019.



- 535 Rigby, M., Prinn, R. G., Fraser, P. J., Simmonds, P. G., Langenfelds, R. L., Huang, J., Cunnold, D. M.,
Steele, L. P., Krummel, P. B., Weiss, R. F., O'Doherty, S., Salameh, P. K., Wang, H. J., Harth, C. M.,
Mühle, J., and Porter, L. W.: Renewed growth of atmospheric methane, *Geophysical Research Letters*,
35, L22805, 10.1029/2008gl036037, 2008.
- Rigby, M., Montzka, S. A., Prinn, R. G., White, J. W. C., Young, D., O'Doherty, S., Lunt, M. F., Ganesan,
540 A. L., Manning, A. J., Simmonds, P. G., Salameh, P. K., Harth, C. M., Muhle, J., Weiss, R. F., Fraser, P.
J., Steele, L. P., Krummel, P. B., McCulloch, A., and Park, S.: Role of atmospheric oxidation in recent
methane growth, *Proc Natl Acad Sci U S A*, 114, 5373-5377, 10.1073/pnas.1616426114, 2017.
- Rowlinson, M. J., Rap, A., Arnold, S. R., Pope, R. J., Chipperfield, M. P., McNorton, J., Forster, P.,
Gordon, H., Pringle, K. J., Feng, W., Kerridge, B. J., Latter, B. L., and Siddans, R.: Impact of El Niño–
545 Southern Oscillation on the interannual variability of methane and tropospheric ozone, *Atmos. Chem.
Phys.*, 19, 8669-8686, 10.5194/acp-19-8669-2019, 2019.
- Saunois, M., Bousquet, P., Poulter, B., Peregon, A., Ciais, P., Canadell, J. G., Dlugokencky, E. J., Etiope,
G., Bastviken, D., Houweling, S., Janssens-Maenhout, G., Tubiello, F. N., Castaldi, S., Jackson, R. B.,
Alexe, M., Arora, V. K., Beerling, D. J., Bergamaschi, P., Blake, D. R., Brailsford, G., Brovkin, V.,
550 Bruhwiler, L., Crevoisier, C., Crill, P., Covey, K., Curry, C., Frankenberg, C., Gedney, N., Höglund-
Isaksson, L., Ishizawa, M., Ito, A., Joos, F., Kim, H. S., Kleinen, T., Krummel, P., Lamarque, J. F.,
Langenfelds, R., Locatelli, R., Machida, T., Maksyutov, S., McDonald, K. C., Marshall, J., Melton, J. R.,
Morino, I., Naik, V., O'Doherty, S., Parmentier, F. J. W., Patra, P. K., Peng, C., Peng, S., Peters, G. P.,
Pison, I., Prigent, C., Prinn, R., Ramonet, M., Riley, W. J., Saito, M., Santini, M., Schroeder, R., Simpson,
555 I. J., Spahni, R., Steele, P., Takizawa, A., Thornton, B. F., Tian, H., Tohjima, Y., Viogy, N., Voulgarakis,
A., van Weele, M., van der Werf, G. R., Weiss, R., Wiedinmyer, C., Wilton, D. J., Wiltshire, A., Worthy,
D., Wunch, D., Xu, X., Yoshida, Y., Zhang, B., Zhang, Z., and Zhu, Q.: The global methane budget 2000–
2012, *Earth Syst. Sci. Data*, 8, 697-751, 10.5194/essd-8-697-2016, 2016.
- Saunois, M., Bousquet, P., Poulter, B., Peregon, A., Ciais, P., Canadell, J. G., Dlugokencky, E. J., Etiope,
560 G., Bastviken, D., Houweling, S., Janssens-Maenhout, G., Tubiello, F. N., Castaldi, S., Jackson, R. B.,
Alexe, M., Arora, V. K., Beerling, D. J., Bergamaschi, P., Blake, D. R., Brailsford, G., Bruhwiler, L.,
Crevoisier, C., Crill, P., Covey, K., Frankenberg, C., Gedney, N., Höglund-Isaksson, L., Ishizawa, M., Ito,
A., Joos, F., Kim, H. S., Kleinen, T., Krummel, P., Lamarque, J. F., Langenfelds, R., Locatelli, R., Machida,
T., Maksyutov, S., Melton, J. R., Morino, I., Naik, V., O'Doherty, S., Parmentier, F. J. W., Patra, P. K.,
565 Peng, C., Peng, S., Peters, G. P., Pison, I., Prinn, R., Ramonet, M., Riley, W. J., Saito, M., Santini, M.,
Schroeder, R., Simpson, I. J., Spahni, R., Takizawa, A., Thornton, B. F., Tian, H., Tohjima, Y., Viogy, N.,
Voulgarakis, A., Weiss, R., Wilton, D. J., Wiltshire, A., Worthy, D., Wunch, D., Xu, X., Yoshida, Y., Zhang,
B., Zhang, Z., and Zhu, Q.: Variability and quasi-decadal changes in the methane budget over the period
2000–2012, *Atmos. Chem. Phys.*, 17, 11135-11161, 10.5194/acp-17-11135-2017, 2017.
- 570 Saunois, M., Stavert, A. R., Poulter, B., Bousquet, P., Canadell, J. G., Jackson, R. B., Raymond, P. A.,
Dlugokencky, E. J., Houweling, S., Patra, P. K., Ciais, P., Arora, V. K., Bastviken, D., Bergamaschi, P.,



- 575 Blake, D. R., Brailsford, G., Bruhwiler, L., Carlson, K. M., Carrol, M., Castaldi, S., Chandra, N.,
Crevoisier, C., Crill, P. M., Covey, K., Curry, C. L., Etiope, G., Frankenberg, C., Gedney, N., Hegglin, M.
I., Höglund-Isakson, L., Hugelius, G., Ishizawa, M., Ito, A., Janssens-Maenhout, G., Jensen, K. M., Joos,
F., Kleinen, T., Krummel, P. B., Langenfelds, R. L., Laruelle, G. G., Liu, L., Machida, T., Maksyutov, S.,
McDonald, K. C., McNorton, J., Miller, P. A., Melton, J. R., Morino, I., Müller, J., Murgia-Flores, F.,
Naik, V., Niwa, Y., Noce, S., O'Doherty, S., Parker, R. J., Peng, C., Peng, S., Peters, G. P., Prigent, C.,
Prinn, R., Ramonet, M., Regnier, P., Riley, W. J., Rosentreter, J. A., Segers, A., Simpson, I. J., Shi, H.,
580 Smith, S. J., Steele, L. P., Thornton, B. F., Tian, H., Tohjima, Y., Tubiello, F. N., Tsuruta, A., Viovy, N.,
Voulgarakis, A., Weber, T. S., van Weele, M., van der Werf, G. R., Weiss, R. F., Worthy, D., Wunch, D.,
Yin, Y., Yoshida, Y., Zhang, W., Zhang, Z., Zhao, Y., Zheng, B., Zhu, Q., Zhu, Q., and Zhuang, Q.: The
Global Methane Budget 2000-2017, *Earth Syst. Sci. Data Discuss.*, 2019, 1-136, 10.5194/essd-2019-128,
2019.
- 585 Turner, A. J., Frankenberg, C., Wennberg, P. O., and Jacob, D. J.: Ambiguity in the causes for decadal
trends in atmospheric methane and hydroxyl, *Proc Natl Acad Sci U S A*, 114, 5367-5372,
10.1073/pnas.1616020114, 2017.
- Turner, A. J., Fung, I., Naik, V., Horowitz, L. W., and Cohen, R. C.: Modulation of hydroxyl variability
by ENSO in the absence of external forcing, *Proceedings of the National Academy of Sciences*, 115,
8931-8936, 10.1073/pnas.1807532115, 2018.
- 590 Turner, A. J., Frankenberg, C., and Kort, E. A.: Interpreting contemporary trends in atmospheric methane,
Proceedings of the National Academy of Sciences, 116, 2805-2813, 10.1073/pnas.1814297116, 2019.
- Wolter, K., and Timlin, M. S.: El Niño/Southern Oscillation behaviour since 1871 as diagnosed in an
extended multivariate ENSO index (MEI.ext), *International Journal of Climatology*, 31, 1074-1087,
10.1002/joc.2336, 2011.
- 595 Yienger, J. J., and Levy II, H.: Empirical model of global soil-biogenic NO_x emissions, *Journal of
Geophysical Research: Atmospheres*, 100, 11447-11464, 10.1029/95jd00370, 1995.
- Zhang, T., Hoell, A., Perlwitz, J., Eischeid, J., Murray, D., Hoerling, M., and Hamill, T. M.: Towards
Probabilistic Multivariate ENSO Monitoring, *Geophysical Research Letters*, 46, 10532-10540,
10.1029/2019gl083946, 2019.
- 600 Zhang, Z., Zimmermann, N. E., Calle, L., Hurtt, G., Chatterjee, A., and Poulter, B.: Enhanced response
of global wetland methane emissions to the 2015–2016 El Niño-Southern Oscillation event,
Environmental Research Letters, 13, 074009, 10.1088/1748-9326/aac939, 2018.
- Zhao, Y., Saunio, M., Bousquet, P., Lin, X., Berchet, A., Hegglin, M. I., Canadell, J. G., Jackson, R. B.,
Hauglustaine, D. A., Szopa, S., Stavert, A. R., Abraham, N. L., Archibald, A. T., Bekki, S., Deushi, M.,
605 Jöckel, P., Josse, B., Kinnison, D., Kirner, O., Maréchal, V., O'Connor, F. M., Plummer, D. A., Revell, L.
E., Rozanov, E., Stenke, A., Strode, S., Tilmes, S., Dlugokencky, E. J., and Zheng, B.: Inter-model
comparison of global hydroxyl radical (OH) distributions and their impact on atmospheric methane over
the 2000–2016 period, *Atmos. Chem. Phys.*, 19, 13701-13723, 10.5194/acp-19-13701-2019, 2019.



610 Zhao, Y., Saunio, M., Bousquet, P., Lin, X., Berchet, A., Hegglin, M. I., Canadell, J. G., Jackson, R. B.,
Dlugokencky, E. J., Langenfelds, R. L., Ramonet, M., Worthy, D., and Zheng, B.: Influences of hydroxyl
radicals (OH) on top-down estimates of the global and regional methane budgets, *Atmos. Chem. Phys.*
Discuss., 2020, 1-45, 10.5194/acp-2019-1208, 2020.

615 Zheng, B., Chevallier, F., Yin, Y., Ciais, P., Fortems-Cheiney, A., Deeter, M. N., Parker, R. J., Wang, Y.,
Worden, H. M., and Zhao, Y.: Global atmospheric carbon monoxide budget 2000–2017 inferred from
multi-species atmospheric inversions, *Earth Syst. Sci. Data*, 11, 1411-1436, 10.5194/essd-11-1411-2019,
2019.

620 Ziemke, J. R., Oman, L. D., Strode, S. A., Douglass, A. R., Olsen, M. A., McPeters, R. D., Bhartia, P. K.,
Froidevaux, L., Labow, G. J., Witte, J. C., Thompson, A. M., Haffner, D. P., Kramarova, N. A., Frith, S.
M., Huang, L. K., Jaross, G. R., Seftor, C. J., Deland, M. T., and Taylor, S. L.: Trends in global
tropospheric ozone inferred from a composite record of TOMS/OMI/MLS/OMPS satellite measurements
and the MERRA-2 GMI simulation, *Atmos. Chem. Phys.*, 19, 3257-3269, 10.5194/acp-19-3257-2019,
2019.

625

630

635



640 **Figures & Tables**

Table 1. Two-box model inversion experiments.

Inversion experiments	OH variability
Inv_OH_std	Full temporal changes (scaled OH fields)
Inv_OH_cli	Climatology OH (average of 1980-2010)
Inv_OH_var	Year-to-year variation only (detrend OH fields)
Inv_OH_trend	Trend only (remove OH year-to-year variation)

645 **Table 2.** Multi-model mean \pm standard deviation (SD) of annual total OH production (P) and loss (L) in Tmol yr⁻¹ and percentage contribution of each production and loss processes to total OH production and loss estimated with multi-model mean OH fields¹.

Chemical reaction	Mean \pm SD	%
Production	209.3 \pm 11.9	/
O(¹D)+H₂O	96.2 \pm 1.9	46%
NO+HO₂	62.6 \pm 4.1	30%
O₃+HO₂	26.2 \pm 1.9	13%
Other prod	24.2 \pm 7.0	12%
Loss¹	209.3 \pm 11.9	/
CO+OH	82.3 \pm 3.8	39%
CH₄+OH	32.4 \pm 1.4	15%
CH₂O+OH	11.5 \pm 0.5	6%
Isoprene+OH	13.1 \pm 1.4	6%
Other loss	69.9 \pm 4.6	33%

¹ The OH production and loss of the EMAC model are not included in the table since total OH production and loss are not given by the EMAC model.

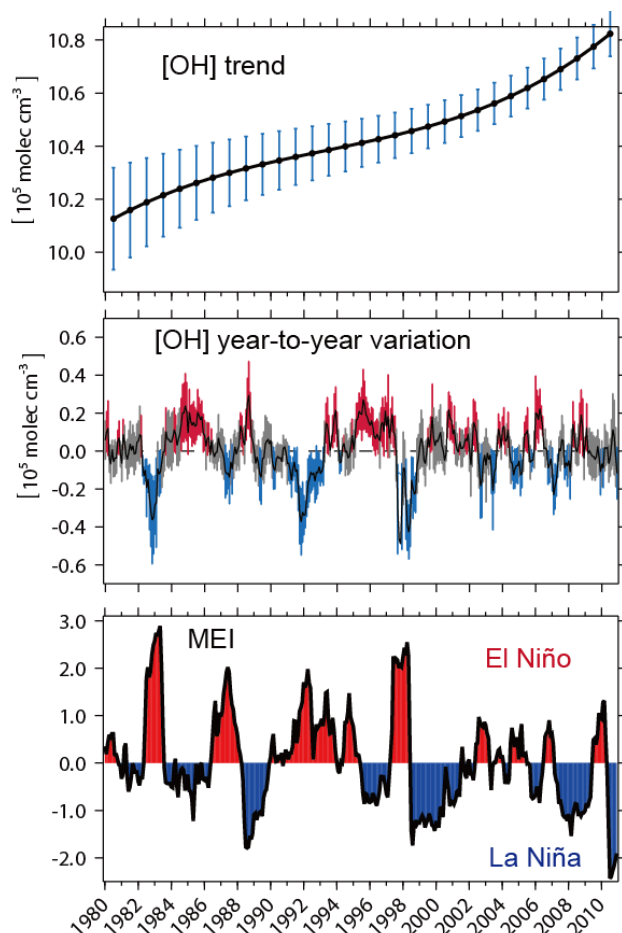


Figure 1. Top panel: Annual global tropospheric mean OH concentration ($[\text{OH}]_{\text{GM-CH}_4}$, CH_4 reaction weighted) with year-to-year variations removed (represents the OH trend) simulated by CCM1 models. The black line is the multi-model mean and associated error bars are standard deviations of different model results (also for the middle panel). Middle panel: Anomaly of detrended and deseasonalized monthly mean $[\text{OH}]_{\text{GM-CH}_4}$ (represents the year-to-year variations of OH). Red bars indicate that the multi-model simulated $[\text{OH}]_{\text{GM-CH}_4}$ are statistically significant ($P < 0.05$) positive anomalies, blue bars indicate statistically significant negative anomalies, and grey bars indicate statistically non-significant anomalies. Bottom panel: Bi-monthly Multivariate ENSO Index (MEI).

655

660

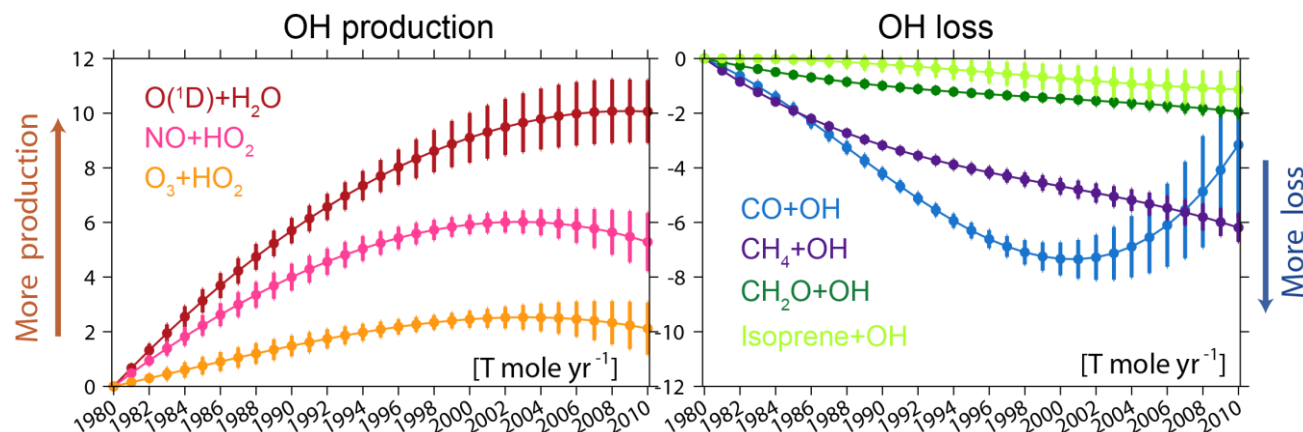


Figure 2. Annual total OH production and loss in Tmole yr^{-1} with respect to the year 1980 with year-to-year variations removed.

665

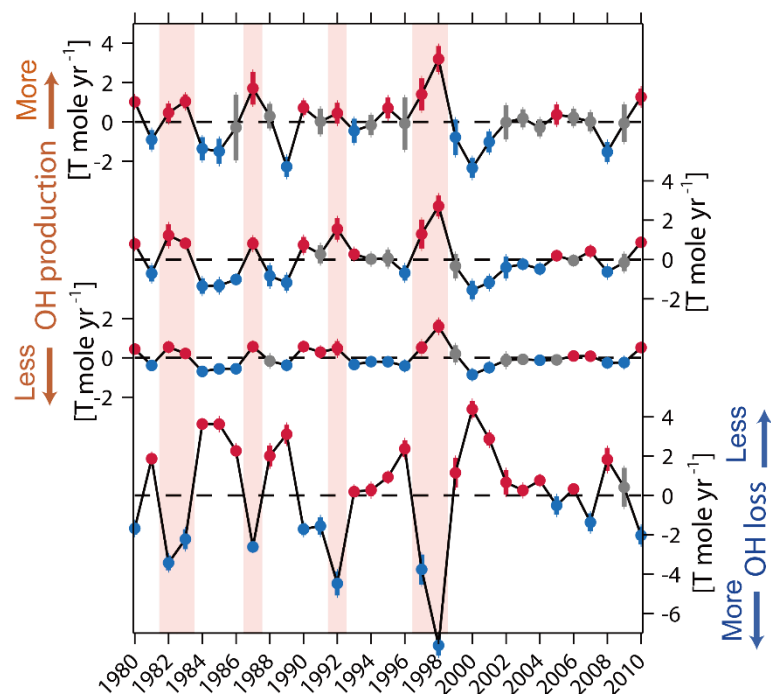
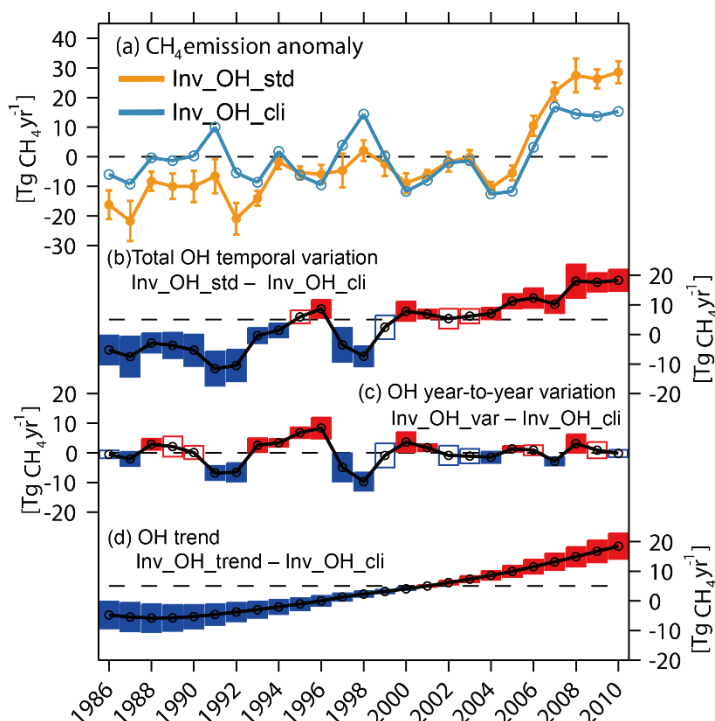


Figure 3. Anomaly of the detrended annual global total OH production from reactions $\text{O}(^1\text{D})+\text{H}_2\text{O}$, $\text{NO}+\text{HO}_2$, O_3+HO_2 , and loss from reaction $\text{CO}+\text{OH}$. Black lines are multi-model means and the error bars are the standard deviations of all CCMI model results. The red, blue, and grey dots and error bars show statistically significant ($P < 0.05$) positive anomalies, negative anomalies, and statistically non-significant anomalies, respectively. Shaded areas represent the El Niño years with more than 5 months of $\text{MEI} > 1.0$.

670



675 **Figure 4.** (a) Anomaly of global total CH₄ emissions using scaled CCMI OH fields (yellow line, Inv_OH_std), and climatological OH (blue, Inv_OH_cli) estimated by a two-box model inversion. The anomalies are calculated by comparing to the climatological mean CH₄ emissions of Inv_OH_cli over 1986-2010. (b) Influence of total OH temporal variations (OH year-to-year variation and trend, Inv_OH_std minus Inv_OH_cli), (c) OH year-to-year variations (Inv_OH_var minus Inv_OH_cli), and
680 (d) OH trend (Inv_OH_trend minus Inv_OH_cli) on box-model estimated global total CH₄ emissions. The black lines are the mean of inversion results with different OH fields and the boxes are ±one standard deviation. The boxes with filled blue/red show OH lead to statistically significant (P<0.05) differences between the two inversions.

685

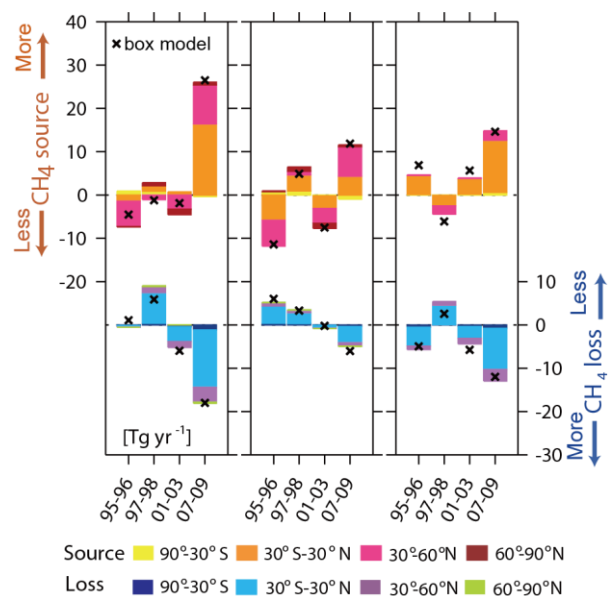


Figure 5. Anomaly of CH₄ emissions and losses estimated by variational 4D inversions (bars) and by two-box model inversions (“x”) using a multi-model mean scaled OH (Inv_OH_std, left column) and climatological OH (middle column) during four time periods. The anomalies are calculated by comparing to the mean CH₄ emissions of Inv_OH_cli over the four time period. The differences between Inv_OH_std and Inv_OH_cli (Inv_OH_std minus Inv_OH_cli) are presented in the right column. The total emissions and loss over southern extra-tropical regions (90 °S-30 °S), the tropics (30 °S-30 °N), the northern temperate (30 °-60 °N), and the boreal (60 °-90 °N) regions are shown by different colors within each bar.

690

695

700

705